Journal of Polymers and the Environment (2019) 27:1259–1272
https://doi.org/10.1007/s10924-019-01401-6

ORIGINAL PAPER

Non-isothermal Crystallization and Degradation Kinetics of Fe_3O_4–Thymolblue Functionalized Poly(ε-caprolactone)

S. Mahalakshmi[1] · V. Parthasarathy[2] · Kuo-Lun Tung[3] · R. Anbarasan[3] · T. Alagesan[4]

Published online: 26 March 2019

Abstract

The Fe_3O_4–thymolblue (TB) functionalized or end capped poly(ε-caprolactone) (PCL) was synthesized by ring opening polymerization (ROP) of ε-caprolactone (CL) with Fe_3O_4–TB nanohybrid as an effective initiator in the presence of stannous octoate (SO) as a catalyst. The main aim of the present work is to analyze the influence of polymer chain end capping agent or functionalization agent on the structure–property relationship particularly, crystallization and thermal degradation behavior of PCL under non-isothermal condition. The structure of the polymer was analyzed using FTIR and NMR spectra. The particle size of the incorporated Fe_3O_4–TB nanohybrid in PCL matrix was found to be less than 20 nm by TEM. The surface morphology, skewness moment and surface roughness were analysed by AFM. The spherulitic growth of the nucleated polymer crystals was confirmed by POM. The spherulitic growth was further verified with various kinetic models. The melting and crystallization behaviors under non-isothermal condition were assessed by DSC. Various kinetic models were employed to comprehend the degradation behavior of Fe_3O_4–TB functionalized PCL and its associated kinetic parameters under non-isothermal condition. The energy of activation (E_a) for the crystallization and thermal degradation of PCL were found to be 132 and nearly 140 kJ/mol respectively.

Keywords Kinetics · PCL · Degradation · POM · Spherulite · Crystallization

Introduction

Poly(ε-caprolactone) is a synthetic bio-degradable polyester made up of hexanoate repeating units. It receives much attention than other commercially available biodegradable polyesters owing to its semi-crystalline, oil resistance, hydrolytic degradation, biocompatible and biodegradable properties [1, 2]. The applications of PCL are innumerable such as the development of surgical sutures, implants, bio-renewable items, bio-resorbable devices and composite bags for some biomedical applications, and also in pharmaceutical and agricultural sectors [3–5]. PCL is also used in controlled drug delivery due to its high permeability to the wide range of drugs and biocompatibility [6]. PCL has been recognized as the safest polymer for its nontoxic nature to living organisms. The physical properties of PCL mainly depend on its molecular weight and degree of crystallinity. The ROP of CL is the promising method to obtain a polymer with high molecular weight and low polydispersity. The polymerization of CL was carried out using three different tin(II) butoxides by Dumklang et al. [7]. An Eosin Y functionalized multiwalled carbon nanotube (MWCNT) was used as an initiator for ROP of CL [8]. Zinc, magnesium, stannous alkoxides, as well as lanthanide derivatives, were reported as effective initiators for ROP of CL [9–13]. The ROP of CL was initiated by various chemical initiators, calcium mercaptosuccinate [14], sodium hydride [15] and isopropanol [16]. It was found that there is no report on the ROP of CL using TB decorated Fe_3O_4 as an initiator so far in the documented literature. The Fe_3O_4–TB nanohybrid was

✉ V. Parthasarathy
parthu0406@gmail.com

✉ Kuo-Lun Tung
kltung@ntu.edu.tw

[1] Department of Physics, Anand Institute of Higher Technology, Kazhipattur, Chennai, Tamilnadu 603103, India

[2] Department of Physics, Hindustan Institute of Technology and Science, Padur, Chennai, Tamilnadu 603103, India

[3] Department of Chemical Engineering, National Taiwan University, Taipei 10617, Taiwan

[4] Department of Physics, Presidency College, Chennai, Tamilnadu 600005, India

prepared and used as an effective initiator for the ROP of CL by our research team.

The potential applications of PCL are mainly in the biomedical engineering field. The crystallization and morphological properties of PCL are more important than its above-said properties for this application. The final properties of semi-crystalline PCL depend on its crystalline fraction, which gets affected by the crystallization condition. Hence, the study on the crystallization of PCL under the non-isothermal condition is being received more practical significance, as most of the processing techniques are melt based, which takes place only under non-isothermal conditions. Non-isothermal crystallization kinetics of PCL was reported in the literature [17]. The polarized optical microscope (POM) was used to confirm the spherulitic morphology of both PCL and its bio-composites. The crystallization behavior of PCL was studied under both isothermal and non-isothermal conditions [18]. The PCL and PCL/glass composites were investigated under non-isothermal condition [19]. The kinetic parameters associated with the crystallization process were determined by using Mo's and Jeziorny methods. The crystallization mechanism, nucleation and morphology of PCL-graphene oxide composites under non-isothermal conditions were reported by many researchers [20, 21]. The crystallization and melting behavior of PCL/MWCNT composites were examined under both isothermal and non-isothermal conditions [22]. PCL undergoes slight degradation during an industrial process while processing it under the non-isothermal condition, which in turn affects the material's properties. Therefore, the understanding of thermal degradation process of PCL and its composites under the non-isothermal condition is very useful to prepare materials for particular applications. Persenaire et al. [23] studied the mechanism and kinetics of thermal degradation of PCL. The energy of activation for the thermal decomposition process was determined. The thermal stability and decomposition kinetics of PCL/nanoclay were investigated using TGA [24]. It was reported that the activation energy associated with the thermal decomposition process was higher for pure PCL than its composites. The thermal decomposition behavior of starch-based PCL bio-composites was reported by Carmona and co-workers through non-isothermal approach [25]. Also, the associated activation energy for thermal decomposition of the prepared bio-composites was determined by the Ozawa method. The kinetic parameters in connection with the degradation process of PCL biopolymers and its composites were analyzed by a non-isothermal approach using kinetic models [26]. Su and his co-workers [27] investigated the thermal stability of PCL by TGA and its thermal decomposition mechanism by an iterative iso-conversional method. The outcome of the present work is more useful to comprehend the crystallization, melting and thermal degradation behaviors of PCL under non-isothermal condition because these parameters are related with the processing, application and thermal recycling of PCL. The newly prepared Fe_3O_4–TB nanohybrid is not only acting as an initiator for the ROP of CL and also acting as a nucleating agent during the crystallization process of PCL. However, the decrease in T_c can be explained on the basis of segmental mobility and the semi-crystalline nature of PCL. The present investigation brings the new idea about the role of end capping agent or functionalization group on the thermal degradation, morphological and crystallization behavior of PCL.

Experimental

Materials

The chemicals utilized for this experimental work were used as received without further purification. Ferrous sulphate ($FeSO_4$), ferric chloride ($FeCl_3$) and sodium hydroxide (NaOH) were procured from S.D. fine chemicals, India. Thymolblue (TB, initiator) was supplied by Aldrich, India. Chloroform ($CHCl_3$), diethyl ether, ε-caprolactone (CL, monomer, 99.9% pure) and stannous octoate (SO, catalyst, 99% pure) were supplied by Merck, India.

Synthesis of Fe_3O_4–TB Nanohybrid

For the preparation of TB decorated Fe_3O_4 nanohybrid, 1.0 g of TB was dissolved in 50 mL of double distilled water. $FeSO_4$ and $FeCl_3$ (1:2 molar ratio) were separately mixed in a beaker. Both the separately prepared solutions were mixed together under constant stirring at room temperature until that became a homogeneous solution. Afterwards, NaOH solution was added into the homogeneous mixture until the color of the solution turned as dark black. The reaction was continued further for 2 h under constant stirring. Finally, the obtained black precipitate was separated from the supernatant solution by centrifugation at higher rpm. The separated black precipitate was kept at 100 °C in an oven for drying. Thus obtained final product was TB decorated Fe_3O_4 nanohybrid. The reaction is shown in Scheme 1.

Synthesis of Fe_3O_4–TB Nanohybrid Functionalized PCL

1.0 g CL monomer was taken into a two-way necked thermal reactor (for N_2 inlet and outlet respectively), and that was mixed with the freshly synthesized Fe_3O_4–TB nanohybrid initiator for 10 min at 30 °C under N_2 atmosphere. Here the [M/I] = 400 and the [M/C] = 1000. The homogeneous chemical mixture was kept in an oil bath at 160 °C for 2 h to initiate ROP of CL under nitrogen atmosphere. A highly

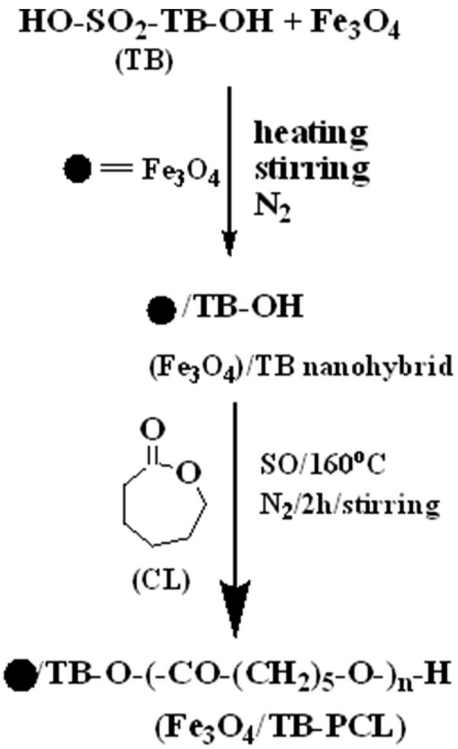

Scheme 1 Synthesis of Fe_3O_4/TB and capped PCL

viscous fluid was obtained at the end of the reaction, which was further dissolved in 15 mL of $CHCl_3$. Afterwards, it was re-precipitated in 200 mL of diethyl ether. Thus prepared black precipitate was Fe_3O_4–TB functionalized PCL. For the preparation of –OH functionalized PCL, 1.0 g of Fe_3O_4–TB functionalized PCL was dissolved in 10 mL of dil. HCl under ultrasonic irradiation for 30 min. Now the contents were filtered to isolate the hydroxyl functionalized PCL from Fe_3O_4–TB nanohybrid.

Characterization of the Sample

The prepared Fe_3O_4–TB functionalized PCL was characterized by various analytical tools to confirm its structure–property relationship. Molecular weight determination of the polymer sample was carried out using gel permeation chromatography (GPC), Perkin Elmer Series 200 in THF solvent and poly(styrene) as an internal standard. FTIR spectral measurement was carried out on Shimadzu 8400S, Japan in the range of 400 to 4000 cm^{-1} to confirm the functional groups present in the Fe_3O_4–TB functionalized PCL. For this measurement, 2 mg of Fe_3O_4–TB functionalized PCL sample was made as a thin pellet by mixing it with 200 mg of KBr under the constant pressure of 7 ton. The chemical structure of the polymer sample was also examined by recording ^1H and ^{13}C-NMR spectra using a 400 MHz JEOL JNM ECS 400 spectrometer in $CDCl_3$ solvent. The surface morphology of the sample was investigated using Park NX10 AFM instrument. The particle size and morphology of the sample was also analyzed by JEOL 2100 HRTEM instrument. The Olympus BX51 optical microscope was used to analyze the crystal growth of the prepared sample. The melting and the crystallization process of Fe_3O_4–TB functionalized PCL were investigated under the non-isothermal condition in the temperature range of – 30 °C to 100 °C at various heating and cooling rates of 10, 15, 20, 25 and 30 °C/min under N_2 atmosphere by using Toledo DSC 822E instrument. Thermal analyser (TG/DTA 6200) was used to analyze the thermal behavior of PCL composite in the temperature range of 30 °C to 600 °C at various heating rates in steps of 5 °C/min.

Non-isothermal Crystallization Kinetics

The various kinetic parameters associated with the crystallization process under non-isothermal condition were obtained from the DSC exothermic curves of the prepared Fe_3O_4–TB functionalized PCL system. Moreover, the heat released during the crystallization process can be calculated by integrating the area under the exothermic curves using DSC. The evolution of crystallinity is directly related with the released heat. Therefore, the relative crystallinity (X_t) is obtained as a function of temperature by the following expression: [28]

$$X_t = \frac{\int_{T_0}^{T} \frac{dH_c}{dT} dT}{\int_{T_o}^{T_\infty} \frac{dH_c}{dT} dT} \quad (1)$$

where dH_c denotes the enthalpy of crystallization, T_0 and T_∞ are the onset and end set crystallization temperatures respectively. The correlation between the crystallization temperature (T) and crystallization time (t) is expressed using the mathematical relation as given below:

$$t = \frac{T_0 - T}{\beta}$$

where β-the cooling rate.

The nucleation mechanism under the non-isothermal condition is well described with the help of the Avrami equation for the PCL system. The Avrami equation is given below:

$$1 - X_t = \exp\left(-Z_t t^n\right) \quad (2)$$

where t is the crystallization time, n is the Avrami exponent which describes nucleation and growth mechanism, Z_t is the crystallization rate constant. Ozawa modified the Eq. (2) and it can also be written as: [29]

$$\ln\left[-\ln\left(1 - X_t\right)\right] = \ln K(T) - m \ln \phi \quad (3)$$

where K(T) is the crystallization rate constant and m-Ozawa index.

The Avrami and Ozawa equations were modified by Mo in order to describe the crystallization parameters under non-isothermal condition. The combined Avrami and Ozawa model suggests the following expression: [30]

$$\log(\Phi) = \log F(T) - b\log(t) \tag{4}$$

where Φ-cooling rate, F(T) is the crystallization rate constant and b is the Ozawa exponent. The exponent b describes the nucleation and the type of the nucleated crystals.

The Kissinger model [31] was also applied to describe the crystallization process under the same condition. It is mainly used to determine the energy of activation for the crystallization process. The following expression was proposed for this model:

$$\frac{d\left[\log\left(\frac{\varphi}{T_c^2}\right)\right]}{d\left(\frac{1}{T_c}\right)} = \frac{E_a}{R} \tag{5}$$

The following equation is obtained by integrating Eq. (5),

$$\log\left(\frac{\varphi}{T_c^2}\right) = \frac{E_a}{R}\frac{1}{T_c} \tag{6}$$

where E_a is the energy of activation, R is the gas constant and T_c is the crystallization temperature at which reaction rate reaches the maximum, and φ is the cooling rate.

The energy of activation is determined by the iso-conversional method. Kissinger–Akahira–Sunose (KAS) is one of the important integral iso-conversional methods. It is used to evaluate activation energies associated with the degree of conversion (α) under non-isothermal condition. This method suggests the following mathematical expression: [32, 33]

$$\ln\left(\frac{\beta}{T_\alpha^2}\right) = -\frac{E_a}{RT_\alpha} + Constant \tag{7}$$

where β is the heating rate, α-degree of conversion, T_α is the temperature associated with the degree of conversion α at various heating rates. According to this method, E_a can be calculated from the slope of the plot $\ln\left(\beta/T_\alpha^2\right)$ vs $1000/T_\alpha$ for each value of the degree of conversion (α) at various heating rates.

Non-isothermal Degradation Kinetics

The kinetic parameters associated with the thermal decomposition of Fe_3O_4–TB functionalized PCL under non-isothermal conditions were analyzed by using four reliable kinetic models. The reaction extent (α) can be proposed by the mathematical relation: [34]

$$\alpha = \frac{W_o - W_t}{W_o - W_f}$$

where W_o is the initial weight of the sample, W_t is the weight at any specified temperature and W_f is the weight of the sample at the end of the process.

Flynn–Wall–Ozawa (FWO) Method

Flynn–Wall–Ozawa (FWO) method [27] deals with the measurement of temperature (T) corresponding to a fixed value of the degree of conversion (α) at different heating rates. The activation energy (E_a) linked with the degradation process can be measured without knowing the reaction mechanism and order using this method. This model suggests the following equation:

$$\ln(\beta) = \ln\frac{AE}{Rg(x)} - 5.331 - 1.052\frac{E}{R}\frac{1}{T} \tag{8}$$

where E is the activation energy, β is the heating rate, R is the gas constant. The activation energy can be measured from the plot of β vs 1/T for this model.

Kissinger Model

The Kissinger model [35] assumes that the reaction rate reaches its maximum at thermal degradation temperature (T_d). Hence, it implies that the degree of conversion (α) is constant at T_d. But, in many cases, the degree of conversion at T_d varies with the heating rate. The Kissinger model proposes the following expression:

$$\ln\left(\frac{\beta}{T_d^2}\right) = \ln\left(\frac{AR}{Ea}\right) - \frac{E}{RT_d} \tag{9}$$

The E_a for the degradation process of functionalized PCL can be evaluated from the plot of $\ln(\beta/T_d^2)$ vs $1/T_d$.

Auggis–Bennet Model

The Auggis–Bennet model [36] is also known as a classical kinetic model. The activation energy for thermal decomposition under non-isothermal condition can also be estimated by this model. This model expresses the following relation:

$$\ln\left(\frac{\beta}{T_d}\right) = -\frac{Ea}{RT_d} + ln\,A \tag{10}$$

where T_d is the degradation temperature. The E_a can be computed by measuring the slope from the plot of $\ln(\beta/T_d)$ vs $1/T_d$.

Friedman Method

The Friedman method is one of the iso-conversional methods [27]. The thermal decomposition mechanism of PCL can be analyzed by the following Arrhenius equation-based mathematical expression:

$$\ln\left(\frac{d\alpha}{dt}\right) = \ln(Z) + n\ln(1-\alpha) - \frac{E_a}{R_1} \quad (11)$$

where R is the gas constant, α is the conversion rate at time t. The plot of ln(dα/dt) vs 1/T is required to estimate E_a values at different stages of degradation reaction.

Results and Discussion

For the sake of convenience, the results and discussion part is sub-divided into three parts, namely, (i) Characterization of Fe_3O_4–TB functionalized PCL, (ii) Non-isothermal crystallization kinetic study of Fe_3O_4–TB functionalized PCL and (iii) Non-isothermal degradation kinetic study of Fe_3O_4–TB functionalized PCL.

(i) Characterization of Fe_3O_4–TB Functionalized PCL

FTIR Spectra and GPC Study

The FTIR spectra of Fe_3O_4, Fe_3O_4–TB nanohybrid and Fe_3O_4–TB functionalized PCL are shown in Fig. 1. Figure 1a indicates the FTIR spectrum of pure Fe_3O_4. The spectrum shows two peaks corresponding to the O-H stretching (3446 cm^{-1}) and the metal oxide (M–O) stretching (598 cm^{-1}) of Fe_3O_4. The FTIR spectrum of Fe_3O_4–TB nanohybrid is given in Fig. 1b. The –OH stretching vibration is identified at 3420 cm^{-1}. The characteristic peaks of C–H symmetric stretching and antisymmetric stretching vibrations of TB are seen at 2892 and 2952 cm^{-1} respectively. The aromatic C–H stretching is witnessed at 2620 cm^{-1}. The other assigned peaks at 1410 cm^{-1} and 1173 cm^{-1} are related to C–S and C–O–C stretching vibrations of TB respectively. The C=C, C–S and $–SO_2$ stretching of TB were observed at 1462 cm^{-1}, 1176 cm^{-1} and 1238 cm^{-1} respectively. The M–O stretching is noticed at 602 cm^{-1} [37]. The FTIR spectrum of Fe_3O_4–TB functionalized PCL is illustrated in Fig. 1c. The O-H stretching vibration of PCL has appeared at 3336 cm^{-1}. The peaks observed at 2863 and 2943 cm^{-1} are assigned to the C–H symmetric and asymmetric stretching vibrations respectively. The carbonyl group (C=O) of PCL is noticed at 1718 cm^{-1} [37]. The C–O–C stretching vibration of PCL is found to be at 1174 cm^{-1}. The peak at 722 cm^{-1} is linked with the C–H out of plane bending vibration of PCL. The M–O stretching has appeared at 596 cm^{-1}. However, the presence of C–H and C=O stretching characteristics peaks are mainly used to confirm the functionalities of PCL.

The chemical polymerization of CL in the presence of Fe_3O_4–TB nanohybrid was confirmed by GPC measurement. The GPC profile of pure PCL and Fe_3O_4–TB functionalized PCL are portrayed in Fig. 1d, e respectively. The results of the profiles revealed that the weight average molecular weight (M_w) of Fe_3O_4–TB functionalized PCL

Table 1 GPC data of pure PCL and Fe_3O_4–TB functionalized PCL

System	M_n	M_w (g/mol)	P.D
PCL	11,532	13,682	1.18
Fe_3O_4–TB–PCL	12,118	14,556	1.2

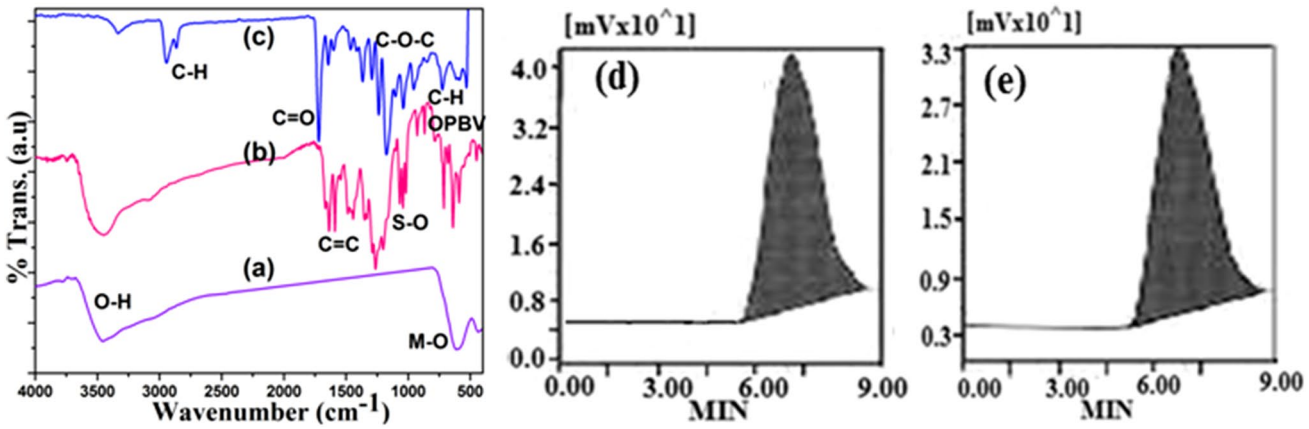

Fig. 1 FTIR spectra of **a** Fe_3O_4, **b** Fe_3O_4–TB nanohybrid, **c** Fe_3O_4–TB functionalized PCL system and GPC trace of **d** pure PCL and **e** Fe_3O_4–TB functionalized PCL

was considerably higher than pure PCL. The rise in the molecular weight of the Fe_3O_4–TB functionalized PCL is due to the attached nanohybrid end groups with PCL. The GPC data are listed in Table 1.

NMR Study

The chemical structure of Fe_3O_4–TB functionalized PCL was examined with the help of ^{1}H- and ^{13}C-NMR spectra. The ^{1}H-NMR spectrum of Fe_3O_4–TB functionalized PCL is displayed in Fig. 2a. The solvent peak of $CDCl_3$ is observed at 7.3 ppm. The alkoxy proton peak is seen at 4.17 ppm in the ^{1}H-NMR spectrum [38]. The signal at 2.30 ppm is associated with the methylene proton of PCL located to the near by carbonyl group. The assigned signals between 1.37 and 1.7 ppm are witnessed to other methylene protons of PCL. The structure of PCL was confirmed by the above discussed peaks. The ^{13}C-NMR spectrum of Fe_3O_4–TB functionalized PCL is mentioned in Fig. 2b. The solvent signals are observed between 76.5 and 77.4 ppm in the ^{13}C-NMR. A peak at 173.1 ppm is referred to the carbon signal of the carbonyl group of PCL [34]. The alkoxy carbon signal peak is assigned at 64.4 ppm. The signal for methylene carbon adjacent to the carbonyl group of PCL is seen at 34.01 ppm. The chemical structure of Fe_3O_4–TB functionalized PCL was confirmed by carbon NMR spectrum.

HRTEM and AFM Study

The HRTEM micrograph of Fe_3O_4–TB functionalized PCL is represented in Fig. 3a. The morphology of the incorporated Fe_3O_4–TB nanohybrid in the PCL matrix is found to be more or less spherical in shape. The size of the particles is varied from 5 to 20 nm. The Fe_3O_4–TB nanohybrids are interconnected with each other in the PCL matrix. Also, the particles of Fe_3O_4–TB nanohybrid seem to be embedded well in the PCL matrix. It also confirms the good interaction between the nanohybrid and PCL. The SAED pattern of the prepared sample is given in Fig. 3b. The appearance of well organized concentric circles in the SAED pattern reveals the semi-crystalline nature of PCL.

The surface texture of Fe_3O_4–TB functionalized PCL was analyzed by AFM. The nature of the material surface can be confirmed with the help of the AFM image. The functional performance of the material is related to the material's surface texture. The surface roughness and grain orientation of PCL was examined using 2D and 3D micrographs (Fig. 3a, b). The presence of well-scattered sharp peaks on the sample surface confirms the interaction of Fe_3O_4–TB with PCL matrix. Moreover, the grains are found to have different size and spacing. The particle size of the Fe_3O_4–TB nanohybrid is found to be less than 20 nm (Fig. 3c). The root mean square and average surface roughness were measured as 7.1 nm and 5.6 nm

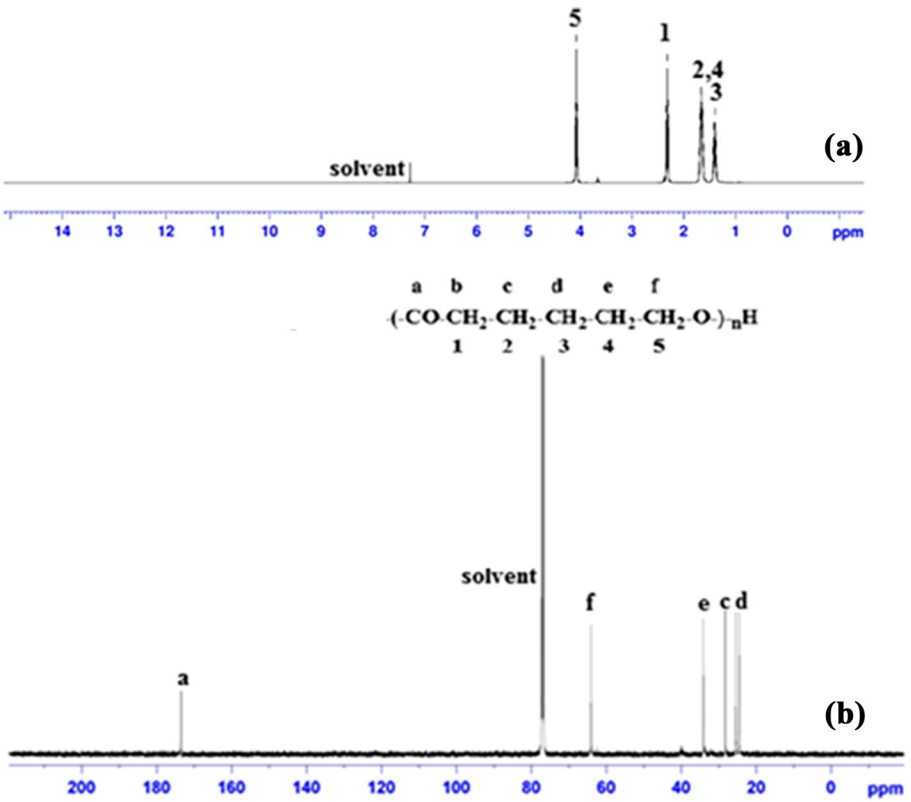

Fig. 2 **a** ^{1}H-NMR and **b** ^{13}C-NMR spectra of Fe_3O_4–TB functionalized PCL

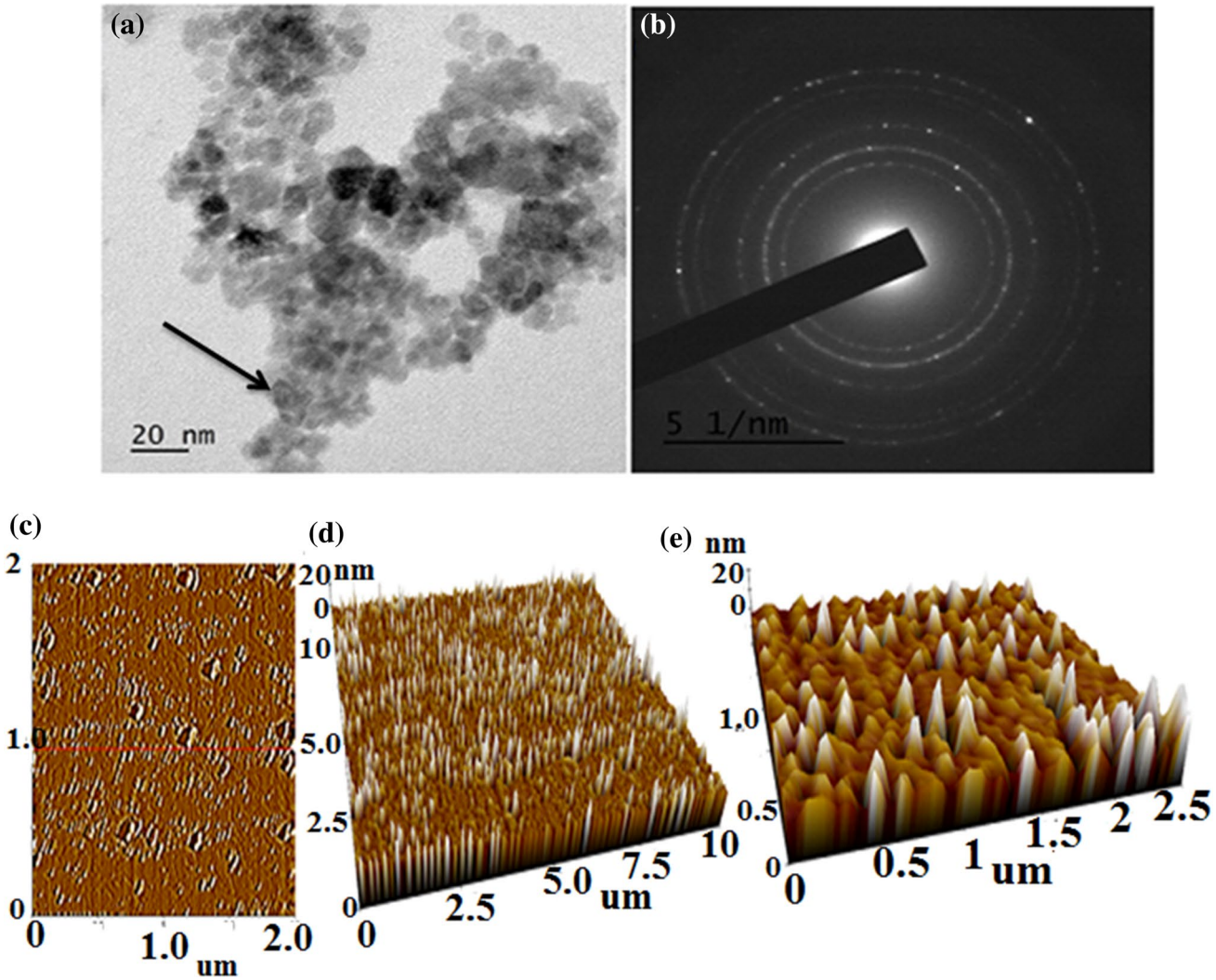

Fig. 3 **a** HRTEM image, **b** SAED pattern of Fe_3O_4–TB functionalized PCL system and **c** 2D AFM image, **d** 3D AFM image (10 µm), **e** 3D AFM image (2.5 µm) of Fe_3O_4–TB functionalized PCL system

respectively. The surface is having both peaks and valleys. However, the surface has more planar region than peaks which is confirmed by the negative Skewness moment (− 0.12). The distribution of peak's height is symmetrical in the 3D micrograph.

(ii) Non-isothermal Crystallization Kinetic Study of Fe_3O_4–TB Functionalized PCL

DSC Profile

The melting and crystallization of PCL were examined under non-isothermal condition by DSC measurement. The DSC heating scan of pure PCL heated at 10 °C/min is displayed in Fig. 4. The T_m of pure PCL (62.7 °C) was lower while compared with T_m of Fe_3O_4–TB

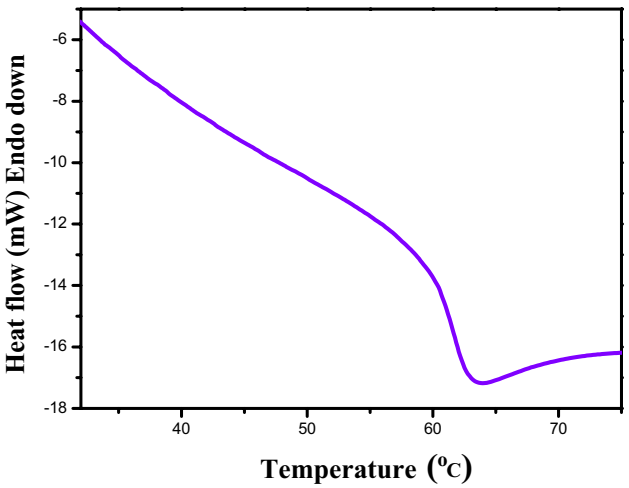

Fig. 4 DSC heating scan of pure PCL

functionalized PCL (66.4 °C) heated at the same heating rate. The increase in T_m is mainly due to the end capped Fe_3O_4–TB nanohybrid in PCL matrix. The melting and crystallization behaviors of Fe_3O_4–TB functionalized PCL were examined by the non-isothermal approach. The Fe_3O_4–TB functionalized PCL was heated in the temperature range of -30 °C to 100 °C at five different heating rates (from 10°C/min to 30 °C/min in steps of 5 °C/min) in N_2 atmosphere (Fig. 5a–e). The sample heated at 10°C/min exhibits a broad peak at 66.4 °C which is corresponding to the T_m of PCL. It was noticed that the T_m of PCL shifts toward higher temperature in accordance with the heating rates. This is in good agreement with the literature report [39]. The increase in T_m with the increase in heating rate was understood from the plot of heating rate vs T_m for Fe_3O_4–TB functionalized PCL (Fig. 5f). The amount of heat energy required for melting the substance was reduced under fast scanning process. The DSC cooling scans of Fe_3O_4–TB functionalized PCL recorded at five different cooling rates are shown in Fig. 5g–k. The crystallization temperature was identified at 30.2 °C for the sample heated at 10 °C/min. It was understood that the T_c value was notably decreased from 30.2 to 24.4 °C while increasing the cooling rates [40]. The plot of cooling rate against T_c is shown in Fig. 5l. The decreasing trend in T_c can be understood from the plot. It concludes that the T_c value of Fe_3O_4–TB functionalized PCL was disturbed while changing the cooling rate. The obtained DSC data is compiled in Table 2.

Non-isothermal Crystallization Study

The crystallization process of Fe_3O_4–TB functionalized PCL was inspected to assess the crystallization rate, nucleation mechanism and the type of crystal growth by the non-isothermal approach. The structure and properties of semi-crystalline PCL depend on the above-said parameters. The prepared PCL was cooled at various cooling rates from 10 °C/min to 30 °C/min in steps of 5 °C/min to comprehend its crystallization behavior. The effect of cooling rates on the crystallization enthalpy (ΔH_c), the degree of crystallinity (X_C) and crystallization peak temperature (T_c)

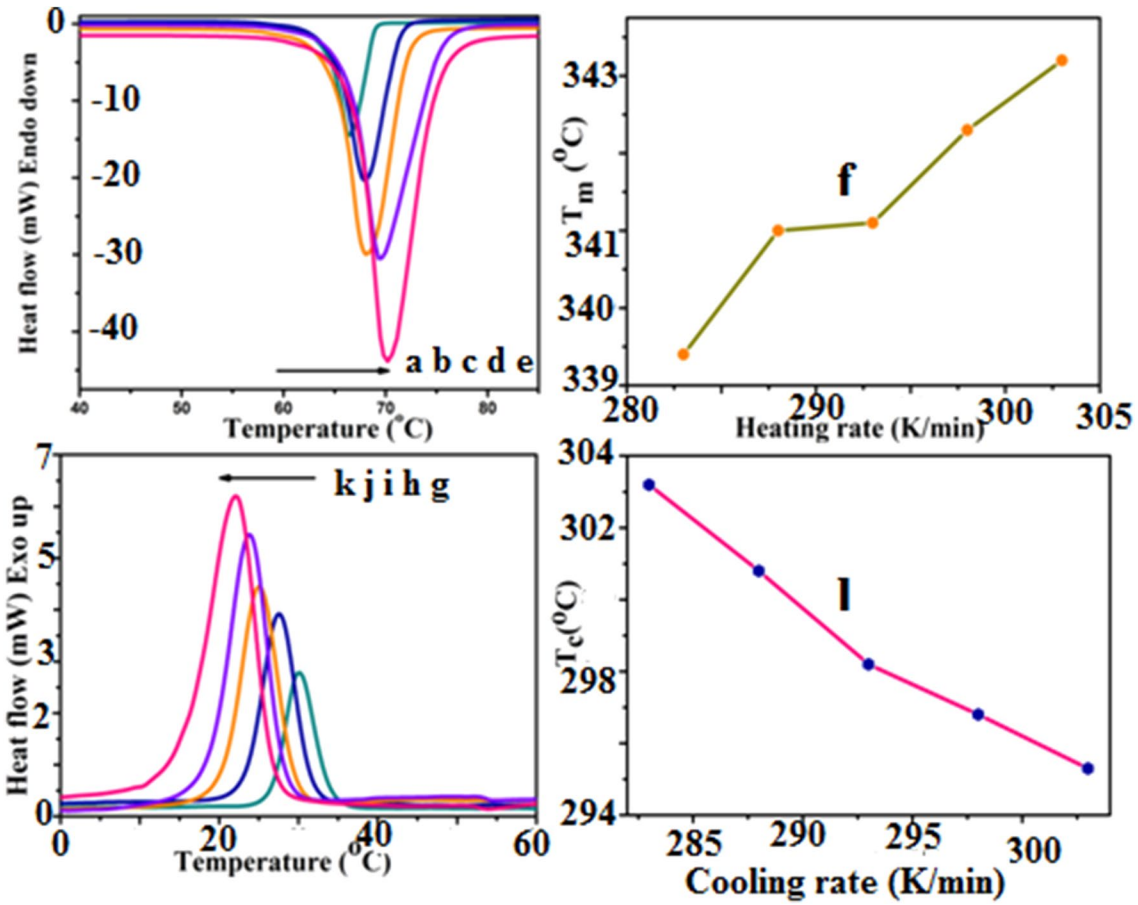

Fig. 5 **a–e** DSC heating scan, **f** plot of heating rate against T_m, **g–k** DSC cooling scan, **l** plot of cooling rate against T_c of Fe_3O_4–TB functionalized PCL system

Table 2 DSC data of Fe_3O_4–TB functionalized PCL

Heating rate (°C)	T_c (°C)	ΔH_c (Jg^{-1})	χ_c (%)	E_a kJ/mol	T_m (°C)	ΔH_m (Jg^{-1})	ΔT ($T_m - T_c$) (°C)
10	30.2	75.8	55.7	132	66.4	95.2	36.2
15	27.8	66.2	48.2		68.0	91.7	40.2
20	25.2	77.3	42.9		68.1	97.3	42.9
25	23.8	71.2	45.5		69.3	89.2	45.5
30	22.3	72.4	47.9		70.2	101.3	47.9

$\chi_c = (\Delta H_f/\Delta H_f^*) \times 100$, ($\Delta H_f^* = 136$ J/g), E_a for the degradation of Fe_3O_4–TB functionalized PCL system

were examined from the crystallization curves as shown in Fig. 4g–k. The crystallization curve becomes broader and the T_c value decreases with the increase in cooling rates. During the cooling process (from the melting stage), the polymer chains are arranged in an ordered and tightly packed fashion. The stereo regular arrangement can be influenced by the chain end capping or functionalization agent. In the present case, the ferrite-TB nanohybrid is an end capping agent. The chain mobility of PCL is restricted by the chain end capping agent. At the higher cooling rate, the PCL chains are tightly packed and arranged in a fast manner. As a result, the T_c values were decreased. Generally, the crystallization process occurs slowly at a lower cooling rate. Therefore, the T_c value shifts toward a higher temperature. While cooling the specimens quickly, more super cooling is required to initiate the crystallization process since the motion of the PCL molecules does not follow the cooling rate.

The nucleation mechanism and growth geometry of the crystals were studied under non-isothermal crystallization condition for the prepared Fe_3O_4–TB functionalized PCL using two different models. According to the proposed Avrami expression in Eq. (3), the Avrami exponent (n) and crystallization rate constant (Z_t) were determined from the

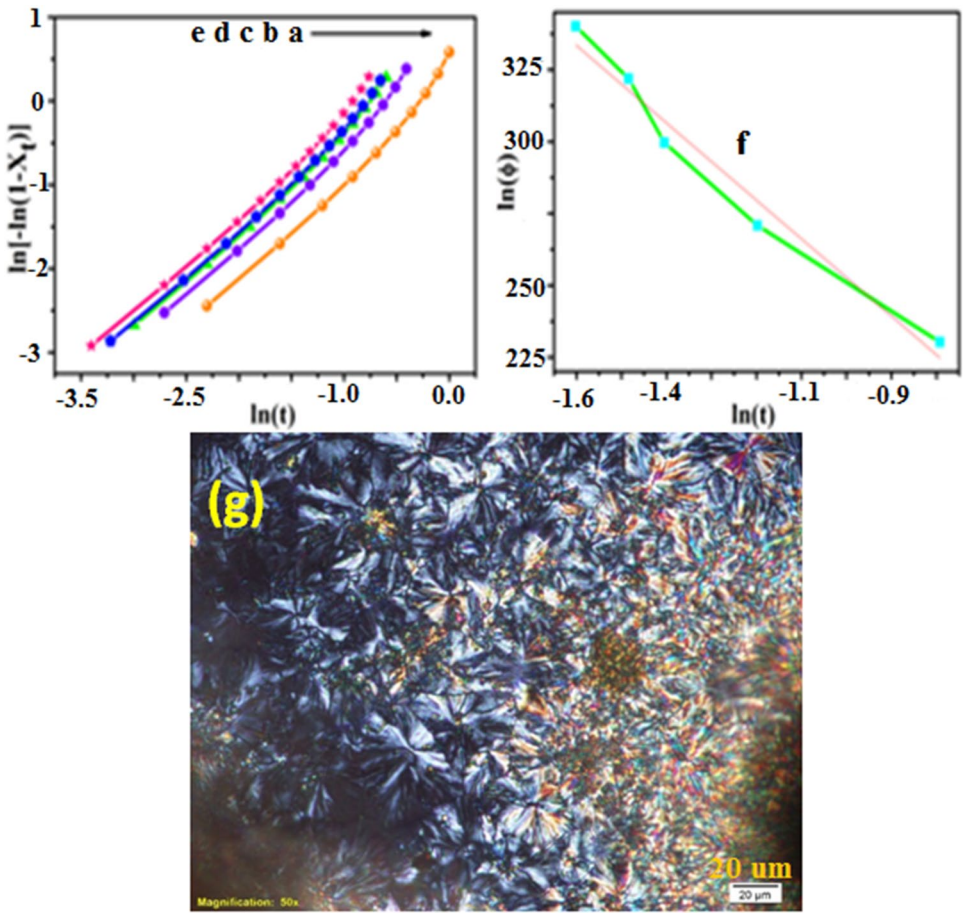

Fig. 6 **a**–**e** Avrami plot for Fe_3O_4–TB functionalized PCL system at the cooling rates of 10, 15, 20, 25, 30 °C min^{-1}, **f** Avrami–Ozawa plot, **g** POM image of Fe_3O_4–TB functionalized PCL system

slope and intercept of the plot of $\ln[-\ln(1-X_t)]$ vs. ln(t) as shown in Fig. 6a-e. The n and Z_t values represent the rate of nuclei formation and the type of growth respectively. The obtained n values were varied from 2.96 to 3.15, which suggested the 3D spherulitic growth [39, 41]. The measured Z_t values were varied from 0.37 to 1.25 for various cooling rates. The crystallization rate increases with the increase in cooling rates. It was concluded that the crystallization rate constant is inversely proportional to crystallization time. The kinetics of Fe_3O_4–TB functionalized PCL was performed by Mo by combining the Avrami and Ozawa equation as given in Eq. (4). The plot of ln(Φ) vs ln(t) was made to calculate the values of F(T) and Ozawa exponent (b) respectively (Fig. 6f). It can be seen that the plot yielded a linear relationship for a given X_t and confirmed that the Mo model can successfully explain the non-isothermal crystallization of ferrite-TB functionalized PCL. In the case of pristine PCL, attainment of such a linear relationship is somewhat difficult because of the absence of functionalization agent or nucleating agent chemically attached with the PCL chains. This explained the role of an end capping agent on the structure–property relationship of PCL. This can be further confirmed by determining the various parameters. The F(T) and b values were obtained as 1.18 and 3.09 respectively. The value of b is above 3, which confirmed the 3D spherulitic crystal growth [37–39]. Hence, both the models authentically confirmed the 3D spherulitic growth as well as the same range of crystallization rate constant for the PCL. The polarized optical micrograph (POM) is illustrated in Fig. 6g. All the grown crystals are in 3D spherulitic shape. Hence, the kinetic results are matched with the experimental result. The POM micrograph shows more number of spherulites per unit area. As a result, one cannot clearly view the growth of the polymer crystals. Moreover, PCL contains more number of chains with ferrite-TB as a chain end capping agent. This induced the crystallization process, at the same time the chain mobility is arrested to some extent. Due to these reasons, the PCL crystal growth is not clearly observed.

The energy required for the crystallization process was determined by Kissinger model. The plot of $\ln(\Phi/T_c^2)$ vs $1/T_c$ (Fig. 7a) was used to determine the E_a value for the crystallization process of Fe_3O_4–TB functionalized PCL. The E_a value was evaluated as 132 kJ/mol. The E_a value was observed to be lower when compared with pure PCL [42]. This is due to the incorporated Fe_3O_4–TB nanohybrid in PCL matrix which considerably enhances the transportation ability of polymer chains during the crystallization process. The crystallization rate coefficient (CRC) was obtained as −0.396 from the plot of crystallization temperature (T_c) vs. cooling rate (Φ) as shown in Fig. 7b. The crystallization rate is higher for polymers with short repeating units than the polymers with longer repeating units. The plot of T_m against T_c (Fig. 7c) reveals a linear relation between them.

The E_a for the crystallization process was also determined by the iso-conversional method. The KAS method was employed to evaluate activation energies associated with a crystallized fraction under non-isothermal condition. The graph of crystallization fraction (α) as a function of temperature was drawn to determine the temperature associated with the degree of conversion for various heating rates as shown in Fig. 8a–e. The obtained α values are listed in Table 3. The E_a value was determined from the plot of $\ln(\beta/T_\alpha^2)$ vs $1000/T_\alpha$ as shown in Fig. 8f–o. The obtained E_a values are given in Table 3. It is well known that ferrite nanocrystal is a good nucleating agent and resulting with an increase in crystallinity and T_c. But in the present study, the ferrite nanocrystals are decorated with TB dye and attached with PCL chains. Hence, the nucleating activity of ferrite is decreased. During the cooling process, the PCL chain mobility is restricted to some extent by the nanohybrid. More number of spherulites are grown but disturbed by the PCL chain mobility. This can be evidenced by the POM image. From this one can come to the conclusion that smaller the size of nucleating agent the better will be the nucleating activity.

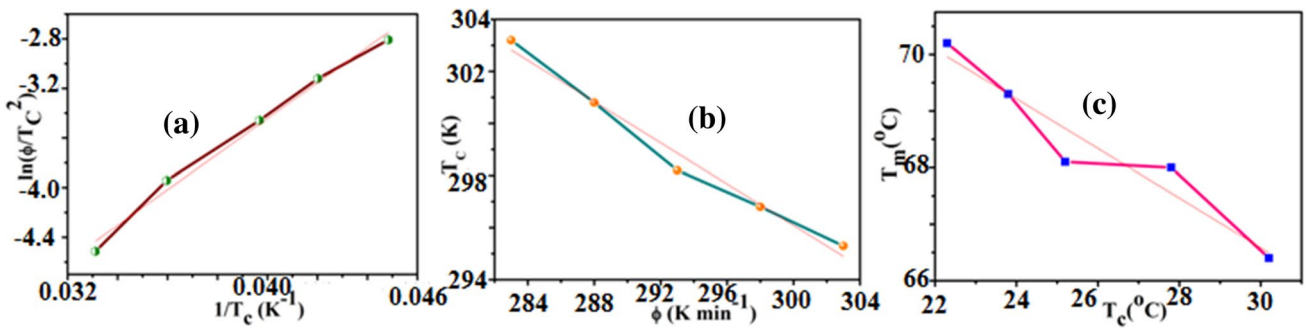

Fig. 7 **a** Kissinger E_a plot, **b** crystallization rate coefficient plot, **c** the plot of T_m against T_c for Fe_3O_4–TB functionalized PCL system

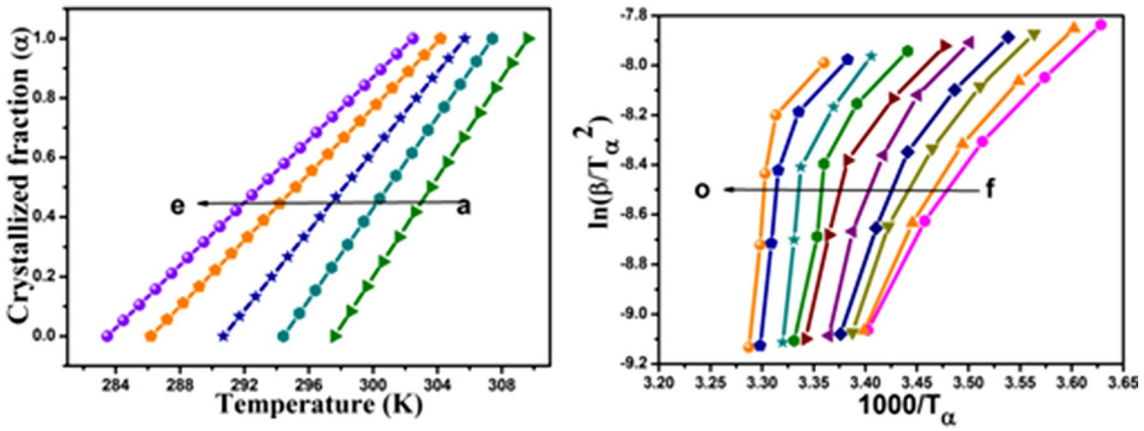

Fig. 8 (**a**–**e**) The plot of temperature against α, (**f**–**o**) KAS plot for the Fe_3O_4–TB functionalized PCL system

Table 3 Determination of E_a values by KAS method for different crystallized fraction of Fe_3O_4–TB functionalized PCL system

Crystallized fraction (α)	Temperature (K/min)					E_a by KAS
	10	15	20	25	30	
0.1	293.9	289.2	284.6	279.8	275.6	44.3
0.2	294.2	290.2	286.2	281.8	277.6	48.6
0.3	295.2	292.2	288.6	284.8	280.6	54.8
0.4	296.2	293.2	290.6	286.8	282.6	59.3
0.5	297.2	295.2	292.6	289.8	285.6	68.7
0.6	299.2	297.2	295.6	291.8	287.6	70.0
0.7	300.2	298.2	297.6	294.8	290.6	82.0
0.8	301.2	300.2	299.6	296.8	293.6	98.5
0.9	303.2	302.2	301.6	299.8	295.6	108.1
1.0	304.2	303.2	303.6	301.8	297.6	118.5

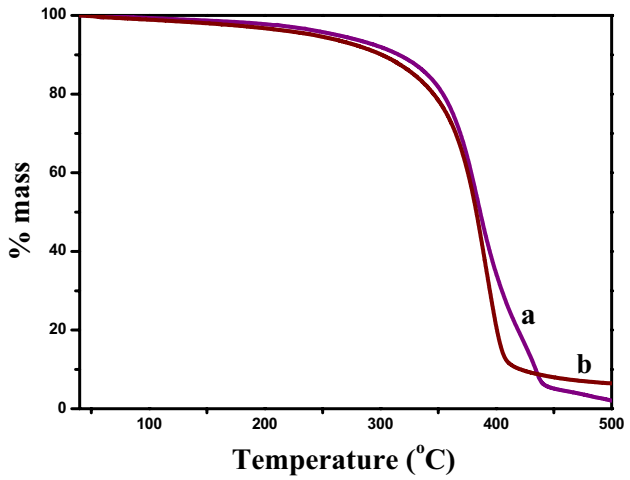

Fig. 9 TG thermogram of **a** pure PCL and **b** Fe_3O_4–TB functionalized PCL

(iii) Non-isothermal Degradation Kinetic Study of Fe_3O_4–TB Functionalized PCL

TGA Profile

The TG thermograms of pure PCL and Fe_3O_4–TB functionalized PCL heated at 10 °C/min are portrayed in Fig. 9a, b respectively. A single step degradation process was perceived for both the systems. The degradation temperature of pure PCL and Fe_3O_4–TB functionalized PCL was determined as 394.8 and 395.5 °C respectively. The thermal stability of the functionalized PCL was slightly enhanced while compared with pure PCL. The thermal stability of Fe_3O_4–TB functionalized PCL was studied under non-isothermal condition. The TG thermograms of Fe_3O_4–TB functionalized PCL was heated in the range of 30 to 600 °C at five different heating rates in the air atmosphere and are shown in Fig. 10a–e. All the thermograms exhibited a single step degradation process

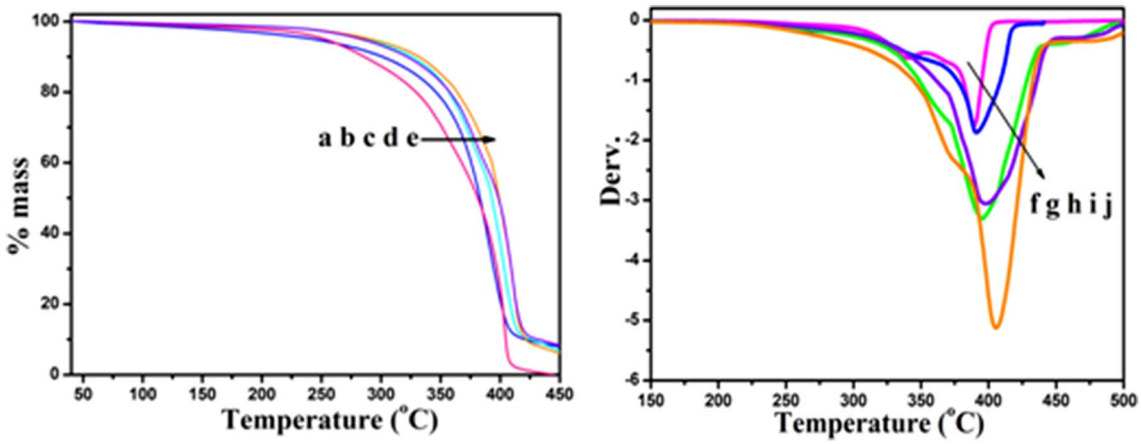

Fig. 10 **a–e** TGA thermograms, **f–j** derivative thermograms of Fe_3O_4–TB functionalized PCL system at five different heating rates

Table 4 TGA data of Fe_3O_4–TB functionalized PCL taken at the heating rate of 10°C/min

System	Onset T_d (°C)	50% T_d (°C)	Maximum T_d (°C)
Pristine PCL	170.3	381.2	388.7
PCL–Fe_3O_4–TB	209.4	387.6	391.1

in the given temperature range for Fe_3O_4–TB functionalized PCL. The decomposition temperature of PCL was found to be shifted to a higher temperature in accordance with the heating rate. This is in good agreement with the literature report [30, 31]. The initial degradation temperature (T_{id}) and the final degradation temperature(T_{fd}) were observed at 240 and 418.3 °C for the functionalized PCL heated at 10 °C/min, which were observed to be increased with the increase in heating rates. The derivative thermograms of Fe_3O_4–TB functionalized PCL for all the heating rates are shown in Fig. 10f–j. The increase in T_d was noticed from the derivative thermograms in accordance with the heating rates. The PEMA-co-PHEMA-g-PCL showed two-step degradation processes with initial degradation temperatures at 243 °C and 361 °C respectively [36]. Hence, the Fe_3O_4–TB functionalized PCL is thermally stable while compared with the previously reported one.

Table 4 showed a comparative TGA data of pristine PCL and Fe_3O_4–TB functionalized PCL systems. The onset, 50% and maximum T_d of Fe_3O_4–TB functionalized PCL system exhibited higher values due to the influence of TB decorated ferrite nanohybrid.

Non-isothermal Degradation Study

The thermal degradation behavior and its associated kinetic parameters under non-isothermal condition were analyzed by four different kinetic models for Fe_3O_4–TB functionalized PCL. The prepared PCL was heated under various heating

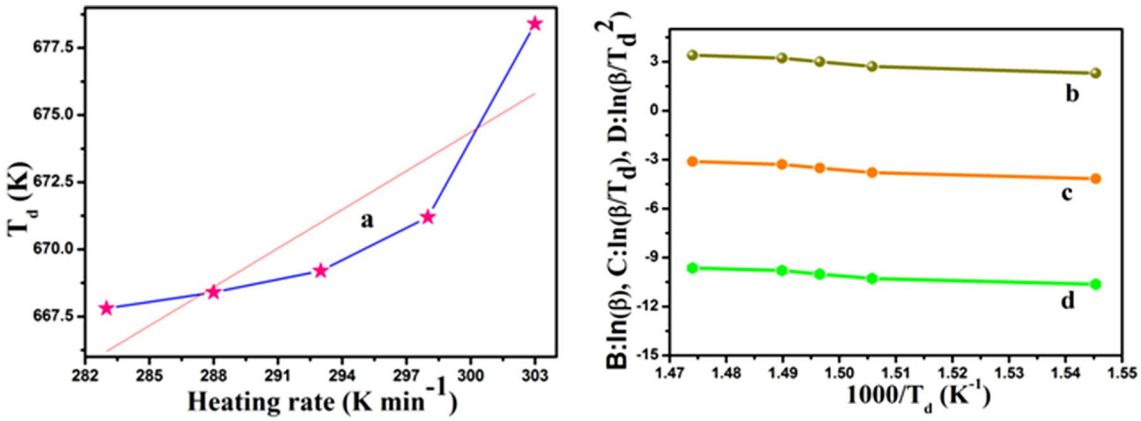

Fig. 11 **a** Effect of heating rate on the T_d of Fe_3O_4–TB functionalized PCL system, **b** Flynnwall–Ozawa plot, **c** Auggis–Bennet plot, **d** Kissinger plot for Fe_3O_4–TB functionalized PCL system

rates in air atmosphere to determine its degradation behavior more accurately. The TGA patterns of Fe_3O_4–TB functionalized PCL and its derivative plots for all the five heating rates are given in Fig. 10a–j respectively. The increase in degradation temperature (T_d) with the increasing heating rates can be understood from the non-isothermal TG and DTG curves. Moreover, the peak area of the DTG curves becomes wider with the increasing heating rates. The plot of T_d vs heating rate (Fig. 11a) revealed the gradual increase in the T_d with the increasing heating rates. This is because of the fast scanning process while heating the specimen. The methodology of finding out E_a for the decomposition process varies with different models. Flynnwall-Ozawa model (the plot of lnβ vs $1000/T_d$; Fig. 11b), Auggis-Bennet method (the plot of $\ln(\beta/T_d)$ vs $1000/T_d$; Fig. 11c) and Kissinger method ($\ln(\beta/T^2_d)$ vs $1000/T_d$; Fig. 11d) were employed to estimate the E_a values for the decomposition process of the PCL [29]. The E_a values were obtained as 146.9 kJ mol^{-1},141.3 kJ mol^{-1} and 138.8 kJ mol^{-1} by Flynnwall–Ozawa, Auggis–Bennet and Kissinger models respectively. The obtained E_a values were in the acceptable error limit only. The E_a value for Kissinger model was lower while comparing with other models.

The Friedman model was implemented to determine the E_a value for the degradation process of Fe_3O_4–TB functionalized PCL. The E_a value was determined from the slope of the plot of $\ln(d\alpha/dt)$ vs 1/T (Fig. 12a–e). A decreasing trend was noticed for all the plots. The calculated E_a values were in the range of 99 to 117.7 kJ mol^{-1} for different heating rates. The plot of E_a vs reaction extent (Fig. 12f) reveals a linear relation between them. The E_a values calculated by Kissinger and Friedman models for Fe_3O_4–TB functionalized PCL were observed to be lower while compared with the reported E_a values (171 kJ mol^{-1} for Kissinger and 177 kJ mol^{-1} for Friedman models) of pure PCL. It was reported that the decrease in E_a was noticed for the PCL/poly(trimethylene carbonate) blend system [34]. Our result is in accordance with the literature report.

The present investigation proved that the size and length of the end capping or functionalization agent can alter the thermal properties of the PCL. When compared with the pristine PCL, the T_c as well as T_d of the Fe_3O_4–TB nanohybrid functionalized PCL has higher values. This is due to the nucleating activity of ferrite nanocrystals. Unfortunately, there is a restriction in the segmental mobility of the PCL offered by the nanohybrid. As a result, there appeared more number of spherulites per unit area.

Conclusion

The Fe_3O_4–TB functionalized PCL was successfully prepared by ROP technique in the presence of Fe_3O_4–TB nanohybrid initiator. The chemical structure of PCL was verified with the help of the observed carbonyl stretching (1720 cm^{-1}) and C–O–C (1179 cm^{-1}) stretching of ester linkage peaks in the FTIR spectrum. The assigned signals at 4.17 ppm and 2.30 ppm in the ^{1}H-NMR spectrum were related to the alkoxy and methylene protons of PCL. The particle size of the incorporated Fe_3O_4–TB nanohybrid was determined to be less than 20 nm. The spherulitic crystal growth was investigated by POM. The Avrami (n) and Ozawa (b) exponents confirmed the 3D spherulitic growth. Hence, the theoretical study was matched with the experimental results obtained. The T_c and T_d of Fe_3O_4–TB functionalized PCL were altered while increasing the heating and cooling rates. The E_a for the decomposition of PCL was evaluated by four different kinetic models. The obtained values were found to be reliable with each other. This study proved that the polymer chain end capping agent can influence the T_c and T_d of the PCL. And it also clearly explained

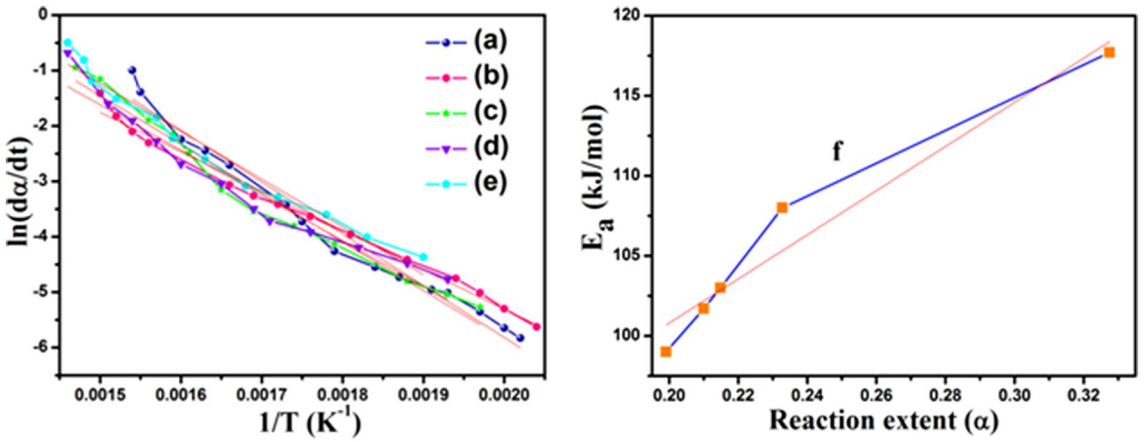

Fig. 12 **a–e** Friedman plot for Fe_3O_4–TB functionalized PCL system at the heating rates of 10 K/min, 15 K/min, 20 K/min, 25 K/min, 30 K/min, **f** plot of E_a against reaction extent

that the size and length of the end capping agent have a definite role while predicting the structure–property relationship of a polymer.

Compliance with Ethical Standards

Conflict of interest There is no conflict of interest among the authors.

References

1. Alamri H, Zhao J, Pahovnik D, Hadjichristidis N (2014) Polym Chem 5:5471
2. Baji ASC, Wong TS, Srivatsan GO, Mathur G (2006) Mater Manuf Process 21:211
3. Castillo RV, Mueller AJ (2009) Prog Polym Sci 34:516
4. Wei X, Gong C, Gou M, Fu S, Guo Q, Shi S, Luo F, Guo G, Qiu L, Qian Z (2009) Int J Pharm 381:1
5. Woodruff MA, Hutmacher DW (2010) Prog Polym Sci 35:1217
6. Fan H, Jin Z (2015) Chem Commun 51:15114
7. Dumklang M, Pattaong N, Punyodom W, Meepowpan P, Molloy R, Hoffman M (2009) Chiang Mai J Sci 36:136
8. Chen H-H, Anbarasan R, Kuo L-S, Chen PH (2011) Mater Chem Phys 126:584
9. Chamberlain BM, Cheng M, Moore DR, Ovitt TM, Lobkovsky EB, Coates GW (2001) J Am Chem Soc 123:3229
10. Shueh ML, Wang YS, Huang BH, Kuo CY, Lin C (2004) Macromolecules 37:5155
11. Storey RF, Sherman JW (2002) Macromolecules 35:1504
12. Kricheldorf HR (2004) J Polym Sci Part A Polym Chem 42:4723
13. Guillaume SM, Schappacher M, Soum A (2003) Macromolecules 36:54
14. Kannammal L, Palanikumar S, Meenarathi B, Anbarasan R (2017) J Thermoplast Compos Mater 30:1056
15. Monelave M, Contreras JM, Laredo E, Carrasquero FL (2010) Express Polym Lett 7:431
16. Darcos V, Habnouni SE, Nottelet B, Ghaoui AE, Coudane J (2010) PolymChem 1:280
17. Yang CT, Lee LT, Wu TY (2018) Polymers 10:543
18. Dhanvijay PU, Shertukde VV, Kalkar AKJ (2012) J Appl Polym Sci 124:1333
19. Oliveira Pires LS, Vaz Fernandes MHF, Marques de Oliveira JM (2018) J Thermal Anal Calorim 134:2115
20. Zhang J, Qiu Z (2011) Ind Eng Chem Res 50:13885
21. Lv Q, Wu D, Qiu Y, Chen J, Yao X, Ding K. Wei N (2015) Thermochim Acta 612:25
22. Tzong-Ming W, Erh-Chiang C (2006) Polym Eng Sci 46:1309
23. Persenaire O, Alexandre M, Degee P, Dubois P (2001) Biomolecules 2:288
24. Hadj-Hamou AS, Metref F, Yahiaoui F (2017) Polym Bull 74:3833
25. Carmona VB, Campos AD, Marconcini JM, Capparelli Mattoso LH (2014) J Therm Anal Calorim 115:153
26. Vangala SPK, Chaudhary A, Tiwari P, Katiyar V (2017) J Energ Environ Sustain 3:10
27. Su TT, Jiang H, Gong H (2008) Polym Plast Technol Eng 47:398–403
28. Mucha M, Tylman M, Mucha J, (2015) Polimery 60:11
29. Tzong MW, Chen EC (2006) Polym Eng Sci 46:1309
30. Li Y, Han C, Yu Y, Xiao L, Shao Y (2018) J Therm Anal Calorim 131:2213
31. Achla S, Maiti N, Jacob J (2017) Int J Polym Anal Ch 22:222
32. Vyazovkin S, Sbirrazzuoli N (2003) J Therm Anal Calorim 72:681
33. Vyazovkin S, Burnham AK, Criado JM, Perez-Maqueda LA, Popescu C, Sbirrazzuoli N (2016) Thermochim Acta 520:1
34. Marquez Y, Franco L, Puiggali J (2012) Thermochim Acta 550:65
35. Reddy MM, Vivekanandhan S, Misra M, Bhatia SK, Mohantty AK (2013) Prog Polym Sci 38:1653
36. Demir P (2017) J Sci Engg 17:73
37. Meenarathi B, Palanikumar S, Kannammal L, Anbarasan R (2015) Spectrochim Acta Part A 35:93
38. Meenarathi B, Chen HH, Chen PH. Anbarasan R (2014) Int J Plast Technol 18:135
39. Mahalakshmi S, Alagesan T, Parthasarathy V, Tung KL, Anbarasan R (2018) J Therm Anal Calorim https://doi.org/10.1007/s10973-018-7514-2. (In Press)
40. Ahmed J, Luciano G, Schizzi I, Ali Arfat Y, Maggiore S, Lidia Arockia Thai T (2018) Thermochim Acta 659:96
41. Kawazu K, Nakagawa S, Ishizone T, Nojima S, Arai D, Yamaguchi K, Nakahama S (2017) Macromolecules 50:7202
42. Vyazovkin S, Sbirrazzuoli N (2006) Macromo Rapid Commun 27:1515